ACS APPLIED MATERIALS & INTERFACES

Research Article

www.acsami.org

Bulk Heterojunction Formation between Indium Tin Oxide Nanorods and $CuInS_2$ Nanoparticles for Inorganic Thin Film Solar Cell Applications

Jin Woo Cho,[†,‡] Se Jin Park,[†] Jaehoon Kim,[†] Woong Kim,[‡] Hoo Keun Park,[§] Young Rag Do,*[,§] and Byoung Koun Min*[,†]

[†]Clean Energy Research Center, Korea Institute of Science and Technology, 39-1 Hawolgok-dong, Seongbuk-gu, Seoul 136-791, Republic of Korea

[‡]Department of Materials Science and Engineering, Korea University, Anam-dong, Seongbuk-gu, Seoul 136-713, Republic of Korea

[§]Department of Chemistry, Kookmin University, Jeongneung-dong, Seongbuk-gu, Seoul 136-702, Republic of Korea

Supporting Information

ABSTRACT: In this study, we developed a novel inorganic thin film solar cell configuration in which bulk heterojunction was formed between indium tin oxide (ITO) nanorods and $CuInS_2$ (CIS). Specifically, ITO nanorods were first synthesized by the radio frequency magnetron sputtering deposition method followed by deposition of a dense TiO_2 layer and CdS buffer layer using atomic layer deposition and chemical bath deposition method, respectively. The spatial region between the nanorods was then filled with CIS nanoparticle ink, which was presynthesized using the colloidal synthetic method. We observed that complete gap filling was achieved to form bulk heterojunction between the inorganic phases. As a proof-of-concept, solar cell devices were fabricated by depositing an Au electrode on top of the CIS layer, which exhibited the best photovoltaic response with a V_{oc}, J_{sc}, FF, and efficiency of 0.287 V, 9.63 mA/cm^2, 0.364, and 1.01%, respectively.

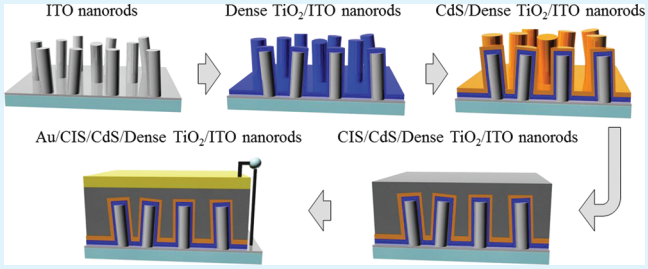

KEYWORDS: *bulk heterojunction, indium tin oxide, ITO, nanorods, $CuInS_2$, solar cells*

INTRODUCTION

Crystalline Si-based solar cells have been successfully used for the efficient conversion of solar energy; however, there is little room for reducing the manufacturing cost, which is a major problem of current electricity production by photovoltaics.[1,2] Even though inorganic thin film solar cells (e.g., $CuInGaSe_2$) have been considered an alternative because of their beneficial optical and physical properties (e.g., high absorption coefficient, stability, etc.), current fabrication methods are not highly cost-effective because vacuum-based processes such as evaporation or sputtering are required.[1,2]

Solution-based fabrication methods of inorganic thin film solar cells may be a candidate for low cost and scalable production of solar cells.[1−4] However, there are several problems associated with solar cell efficiencies of thin film technologies, such as poor material quality (e.g., small crystallites), which results in short photogenerated-carrier diffusion lengths and a high recombination of charge carriers at grain boundaries.[5,6] The crystal size in the film can be increased, but this requires high-temperature treatment processes generally under an extremely toxic gas environment (e.g., H_2Se).[7−9]

Nanoscale heterojunctions may be one solution to this problem because every photogenerated carrier would have less distance to travel to the junction, which will greatly reduce the problem of recombination. Such a bulk heterojunction concept where two interpenetrating charge-conducting networks for charge carriers are constructed has already been shown to be a key technique for achieving highly efficient organic solar cells.[10] The realization of the bulk heterojunction between inorganic phases typically for disordered nanostructures, however, is much more challenging since the achievement of complete gap filling and good electronic contact between the two charge-conducting networks is very difficult.[11−13] For example, TiO_2 films prepared using a paste coating with a sintering process generally resulted in a meso- or nanoporous and disordered three-dimensional network. The solution (e.g., inks) containing p-type semiconductor nanoparticles or precursor ions can be infiltrated into the gaps (or pores) via capillary action followed by removing the solvent by thermal treatment.[14] However, a typical solvent such as water or ethanol has a high surface tension and viscosity; thus, it is difficult for the nanoparticles or precursor ions to reach deep inside of the oxide film, often resulting in incomplete filling of the 3D pore network.[14]

Received: November 1, 2011
Accepted: January 12, 2012
Published: January 12, 2012

The use of ordered nanostructures such as nanorods, nanowires, and nanotubes are more beneficial because more efficient charge collection and transportation can be achieved due to the structural properties of axially grown crystals in the films. To date, several n-type oxide semiconductors (e.g., ZnO and TiO_2) with ordered nanostructures (rods, tubes, wires, etc.) have been used to fabricate organic–inorganic hybrids or extremely thin absorber layer solar cells, which would enhance the performance of solar cells due to the oriented crystalline structure.[15−17] Bulk heterojunction formation between TiO_2 nanotubes and $CuInSe_2$ was achieved using the electrochemical deposition method, although its potential use in solar cell applications was not demonstrated.[12]

In this study, we demonstrate a synthetic strategy (Figure 1) for the novel solar cell configuration in which indium tin oxide

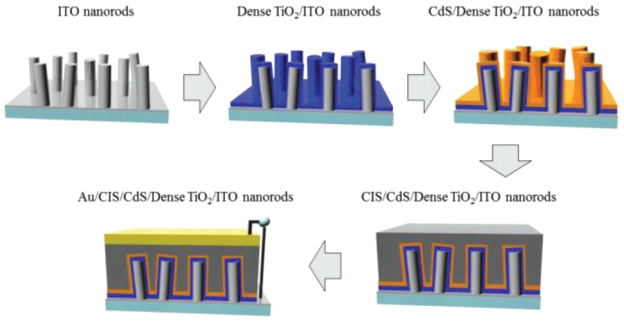

Figure 1. Synthetic scheme of the novel solar cell configuration (Au/CIS/CdS/Dense TiO_2/ITO nanorods) with inorganic phase bulk heterojunction.

(ITO) nanorods were filled with $CuInS_2$ (CIS) using the ink-based deposition method to form an inorganic phase bulk heterojunction. Complete filling of the spatial region of the ITO nanorods with CIS nanoparticles was verified by scanning electron microscopy (SEM) analysis. As a proof-of-concept, solar cell devices were also fabricated and showed a power conversion efficiency of 1.01%.

EXPERIMENTAL SECTION

Materials. Titanium(IV) iso-propoxide (UP Chemical, Korea). Copper chloride (CuCl), indium chloride ($InCl_3$), sulfur (S), oleylamine (OLA), cadmium sulfate ($CdSO_4$), thiourea ($(NH_2)_2CS$), ammonium hydroxide (NH_4OH). All chemicals purchased from sigma-Aldrich.

Preparation of the ITO Nanorod Film. As previously reported in our publication,[22] ITO nanorods were deposited on ITO thin-film coated glass substrates by rf-magnetron sputtering. The ITO thin-film coated glass substrates were ultrasonically cleaned in acetone, ethanol, and deionized (DI) water for 10 min each and dried with N_2 gas. They were then baked at 120 °C for 1 h in a vacuum box. Sputter deposition was carried out in an Ar atmosphere under the following conditions: a background pressure of 2×10^{-6} Torr, a working pressure of 7.8×10^{-3} Torr, and rf-power of 30 W. Three small In metal disks ($d \approx 3$ mm) were placed on a 2 in. ITO target and used as the catalyst for the growth of ITO nanorods. The Sn content (Sn/(In+Sn) atomic ratio) of the target pellet was fixed at 10%. The sputter deposition process was performed at 500 °C for 1 h. After deposition, the sputtering chamber was allowed to cool to room temperature under vacuum. In order to improve the transparency of the ITO nanorods grown on the ITO thin-film coated glass substrate, the post annealing process was carried out at 250 °C for 1 h.

Deposition of the Dense Layer. A ~ 20 nm dense TiO_2 film was deposited on the ITO nanorod film by atomic layer deposition (ALD) at 80 °C. Titanium(IV) iso-propoxide and water vapor, respectively, were used as a metal reactant and oxygen source. Ar was used as the carrier gas and also for the sake of purging. The total flow rate of Ar was 100 cm^3/min. The oxide layers were grown under 2.6 Torr.

Synthesis of CIS Nanoparticles. Chalcopyrite CIS nanocrystals were synthesized by the colloidal synthetic method. The synthetic procedure was carried out in air-free conditions using a Schlenk line. CuCl (0.495 g, 5 mmol) and $InCl_3$ (1.106 g, 5 mmol) were mixed with 50 mL of degassed oleylamine (OLA) in a 100 mL three-neck flask equipped with a condenser. The mixture was purged with Ar gas two times and degassed at 110 °C for 30 min. The temperature of the mixture solution was then increased to 180 °C followed by rapid injection of a solution of S (0.3207 g, 10 mmol) dissolved in 10 mL of OLA. The temperature of the mixture solution was then increased to 240 °C at a heating rate of approximately 10 °C/min, and then maintained for 10 min. After the reaction was complete, the nanocrystal product was precipitated by the addition of ethanol (20 mL), followed by centrifugation at 4500 rpm for 10 min. The isolated nanocrystals were then redispersed in toluene (20 mL) and precipitated again.

Solar Cell Device Fabrication. Solar cell devices with a superstrate-type configuration (ITO nanorod/dense TiO_2/CdS/CIS/Au) were fabricated. ITO nanorods were deposited on the ITO glass substrate by rf-magnetron sputtering. To prepare the dense TiO_2 film on ITO nanorod glass substrates, titanium(IV) iso-propoxide and water vapor were deposited onto the ITO nanorods by ALD. The CdS buffer layers were prepared using the chemical bath deposition (CBD) method from an aqueous solution of $CdSO_4$ (0.1026 g, 0.004 M), $(NH_2)_2CS$ (0.3806 g, 0.05 M) and NH_4OH (15.58 mL, 4 M) at 60 °C. The CdS film deposition time was 7 min. The thickness of the CdS films was varied by controlling the number of deposition processes. CIS films were deposited by a drop-casting method using a premade CIS nanocrystal ink. Finally, an Au electrode film was deposited by a thermal evaporator. For comparison, a planar-type device with superstrate configuration was also fabricated. All fabrication processes were identical to those of the bulk heterojunction device except the use of commercial ITO glass substrates (Samsung Corning, 7 Ω/□) and the preparation method of the dense TiO_2 layer (Sol–gel).[23]

Characterizations. The films were structurally characterized by transmission electron microscopy (TEM, Tecnai G2), scanning electron microscopy (SEM, Hitachi, S-4100), and X-ray diffraction (XRD, Shimadzu, XRD-6000). The optical properties of the CIS nanocrystal inks were measured using a UV–vis spectrometer (Varian, Cary 5000). Composition analysis was carried out by an electron probe microanalyzer (EPMA, Jeol, JXA-8500F) and energy-dispersive X-ray spectroscopy (EDS, EDAX). The solar cell efficiency was measured by a class AAA solar simulator (Sun 2000, Abet Technologies Inc.) and an incident photon conversion efficiency (IPCE) measurement unit (Soma Optics), respectively, under standard irradiation conditions (1.5 A.M., 1 Sun).

RESULTS AND DISCUSSION

First of all, for the transparent conducting oxide layer, ITO nanorods were synthesized using the radio frequency magnetron sputtering deposition method. As shown in the cross-sectional SEM image (Figure 2a), the ITO nanorods were vertically aligned or slightly tilted from the vertical alignment. The approximate thickness and height of the nanorods were measured to be 130 and 700 nm, respectively. The crystal structure of the ITO nanorod film was revealed to be a cubic (bixbyite) structure (see Figure S1 in the Supporting Information), and its sheet resistance and transmittance (at 550 nm) was 8 Ω/□ and 87%, respectively.

A dense layer of TiO_2 was coated on the ITO nanorod film. The dense TiO_2 layer was needed to prevent the formation of an internal shunt due to the leakage currents from direct contact between p-type semiconductor (e.g., CIS) and ITO. In this study, an atomic layer deposition technique was used to

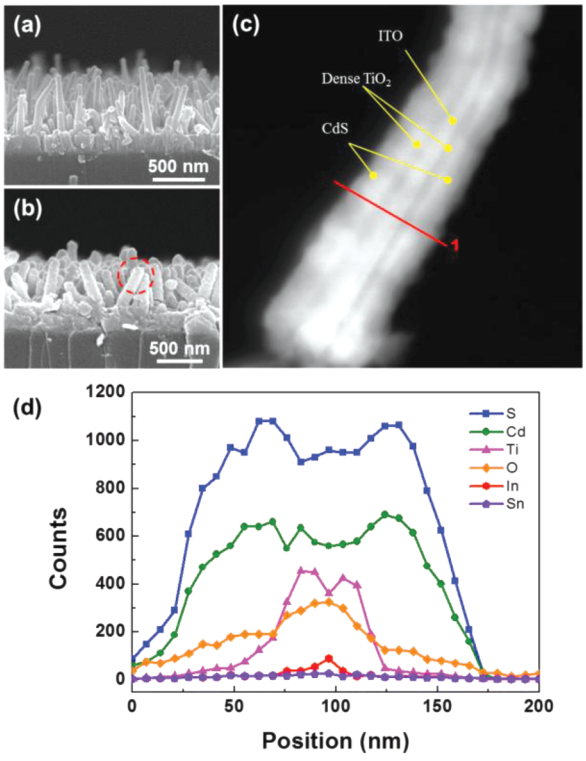

Figure 2. Cross-sectional SEM image of (a) dense TiO_2/ITO nanorods and (b) CdS/dense TiO_2/ITO nanorod, (c) STEM image of a ITO nanorod marked by the circle in b, and (d) EDS elemental analysis through the cross-section of the CdS/Dense TiO_2/ITO nanorod in c (presented by a line 1), which indicates the conformal coating of CdS as well as the TiO_2 layer on the ITO nanorods. The average special distance between the nanorods was 100 nm.

deposit a dense layer of TiO_2.[15,18] As shown in panels c and d in Figure 2, the TiO_2 dense layer was uniformly decorated on the ITO nanorods with a thickness of ~20 nm. Notably, the similar optical property (transmittance) of ITO was observed even after the dense TiO_2 coating (see Figure S2 in the Supporting Information).

Next, a buffer layer was deposited using the chemical bath deposition method. The presence of the buffer layer is also very important because a significant improvement in electronic contact between p-type semiconductor and n-type oxide semiconductor can be achieved.[19] In addition, it is well-known that a buffer layer can be used to avoid shunting of the photocurrent by suppressing the back flow of electrons.[19] In our study, CdS was chosen because it is a commonly used buffer layer material in conventional CIS thin film solar cells. To deposit the CdS onto the dense TiO_2/ITO nanorods, the TiO_2/ITO substrate was immersed in an aqueous solution with Cd and S ions. After the reaction was allowed to proceed at 60 °C for 7 min, the CdS thin film was homogeneously coated on the ITO nanorods as shown in panels b and c in Figure 2. This was further confirmed by element analysis across the rod (Figure 2c, d). The thickness of the CdS layer was measured to be ~50 nm. The most important step in our synthetic processes is filling the gaps between the nanorods with the p-type semiconductor material.

The p-type semiconductor material that we chose was CIS. In general, for conventional CIS thin solar cells, the CIS absorber layer is deposited using the vacuum based method (e.g., coevaporation). However, to produce thin film solar cells in a more cost-effective and scalable way, the solution-based coating method is essential. Therefore, in the present study, we adapted the ink-based coating method (e.g., drop casting) via synthesis of CIS nanoparticles. A synthetic recipe for CIS nanoparticles has already been reported by several research groups.[20,21] Among the methods developed, we were able to prepare dispersed CIS nanoparticles with uniform size (~12 nm) using a slight modified version of the synthetic method described by Hillhouse's group and Korgel's group (Figure 3a).[20,21] These CIS nanoparticles were then redispersed in toluene to form an ink.

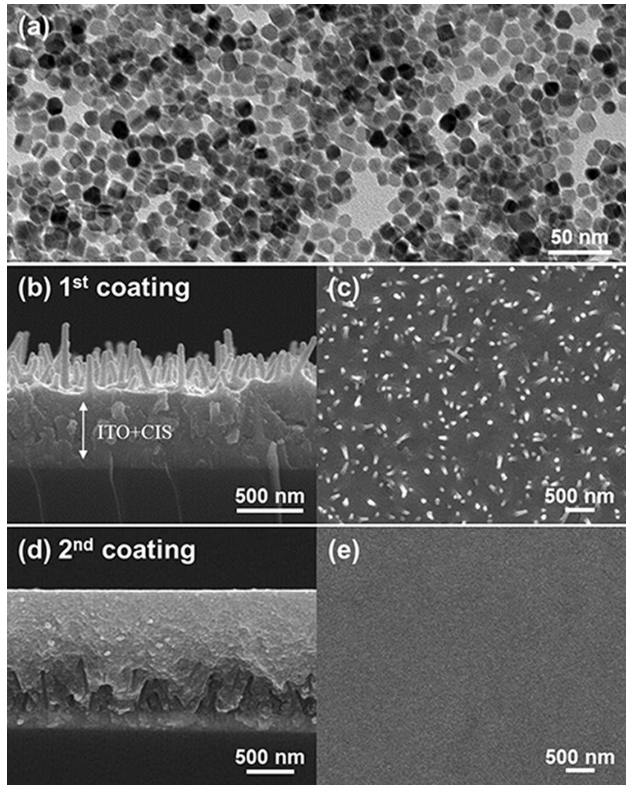

Figure 3. (a) TEM image of CIS synthesized nanoparticles showing well-dispersed nanoparticles with a narrow size distribution. (b, d) Cross-sectional and (c, e) top-view SEM images of the dense TiO_2/ITO nanorod coated by the CIS nanoparticle ink.

One important issue regarding the deposition of the CIS nanoparticle ink into the ITO nanorods template was whether or not the spatial region between the nanorods can be completely filled with CIS nanoparticles. To confirm that gap filling occurred, the CIS nanoparticle ink was discretely drop-casted two times onto the ITO nanorod substrate followed by drying at 120 °C using a hot plate. SEM images of the film were then acquired (Figures 3b-e). Interestingly, as seen in the cross-section SEM image (Figure 3b), the ITO nanorods were half filled with CIS nanoparticles in the first coating step. It was further elucidated in the top-view SEM image in which the heads of the ITO nanorods were still seen (Figure 3c). The second drop-casting step resulted in complete filling of the ITO nanorods, which was confirmed in the cross-sectional as well as the top-view SEM images in (Figure 3d,e).

The same deposition procedure and CIS ink was applied to the ITO nanorods coated by TiO_2 dense as well as CdS buffer layer (see Figure S3 in the Supporting Information). After complete deposition of the CIS nanoparticle ink onto the CdS/

dx.doi.org/10.1021/am201524z | ACS Appl. Mater. Interfaces 2012, 4, 849–853

TiO_2/ITO nanorods film, the sample was annealed at 350 °C under Ar atmosphere to remove residual organic moieties in the film. The CIS nanoparticles were then sintered. Control over the heat treatment conditions is essential because premade layers (e.g., CdS buffer layer and CIS absorber layer) are vulnerable toward high temperature and/or air-conditions. Based on our repeated experiments, the optimum annealing conditions were determined to be 350 °C under an Ar environment. Electron probe microanalyzer (EPMA) analysis confirmed that the amount of carbon impurities was substantially decreased (from 31.7 to 15.9 at%), whereas the composition of Cu, In, and S was not apparently changed. The grain size of the CIS particles, however, was not significantly enhanced under these annealing conditions.

As a proof-of-concept, we fabricated solar cell devices (active area of 0.15 cm^2) by depositing an Au electrode on top of the CIS/CdS/TiO_2/ITO nanorods film. The current density–voltage (J–V) characteristics and the incident photon conversion efficiency (IPCE) showed the best power conversion efficiency of 1.01% at a V_{oc}, J_{sc}, and FF of 0.287 V, 9.63 mA/cm^2, 0.364, respectively (Figure 4). The IPCE data

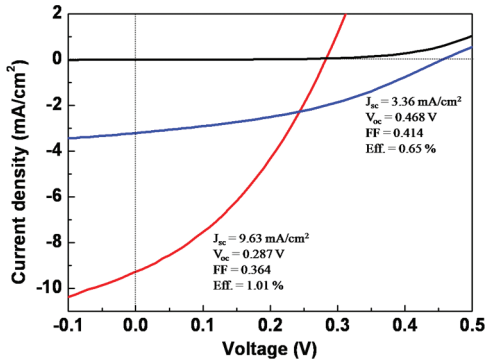

Figure 4. Current density–voltage characteristics of the solar cell devices with inorganic phase bulk heterojunction under dark (black) and light conditions (red, 1.5 A.M. and 1 Sun) and with planar junction for comparison (blue, 1.5 A.M. and 1 Sun).

showed that the photocurrents were generated above 1000 nm wavelength, which was well-matched with the absorbance spectra of the CIS film as shown in Figure 5, implying that the photovoltaic response arises from the CIS film.

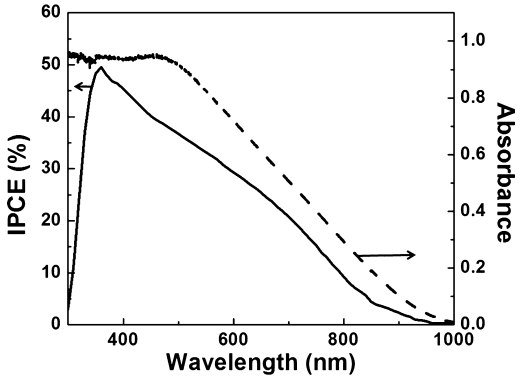

Figure 5. IPCE (solid line) and absorbance (dashed line) spectrum of the solar cell device and the CIS film grown on a soda-lime glass, respectively.

The photovoltaic response of the devices was reproducible, but the efficiencies were still low. Among the many issues (e.g., carbon impurity, Cd diffusion, etc.) that should be improved and optimized in our solar cell device are the V_{oc} and FF, which can be enhanced by minimizing the presence of cracks and/or pores in the CIS film since these factors results in leak currents due to direct contact between the Au electrode and ITO nanorods. The leak currents may also be attributed to the irregular height of ITO nanorods, which induces direct contact between two electrodes. J_{sc} can also be enhanced when the density and/or height of the ITO nanorods is optimized to increase the junction area between CIS and ITO, which is now under investigation in our laboratory.

Finally, to confirm the bulk heterojunction effects on photovoltaic performance, a planar-type device was also fabricated and compared. The planar-type device also had a superstrate configuration (ITO/dense TiO_2/CdS/CIS/Au), and the same CIS ink was applied. Notably, to minimize some possible effects from the thickness of each layer, we made the thickness of each layer almost identical to the bulk heterojunction case (e.g., TiO_2, 100 nm; CdS, 50 nm; and CIS, 800 nm). J–V characteristics showed the power conversion efficiency of 0.65% at a V_{oc}, J_{sc}, and FF of 0.468 V, 3.36 mA/cm^2, 0.414, respectively (Figure 4). In comparison with the J–V characteristics of the bulk heterojunction device, V_{oc} was enhanced whereas J_{sc} was substantially decreased. As a result, overall power conversion efficiency was decreased. Almost 3-fold increase in J_{sc} of the bulk heterojunction device may result from the beneficial effects of the bulk heterojunction formation as we expected. In addition, larger V_{oc} obtained in the planar device gives us an implication that the V_{oc} in the bulk heterojunction device can be also enhanced when some imperfections (e.g., irregular height of ITO nanorods, pores, etc.) of the film are improved.

CONCLUSIONS

In brief, to realize the bulk heterojunction between the inorganic phases, we used ITO nanorod substrate and CIS nanoparticle ink. Nearly complete gap filling of the spatial region between the ITO nanorods was achieved by two times drop-casting of CIS nanoparticle ink onto the ITO nanorod substrate. Incorporation of a dense TiO_2 blocking layer and a CdS buffer layer between ITO and CIS resulted in photovoltaic response of the bulk heterojunction inorganic thin film solar cell devices.

ASSOCIATED CONTENT

Supporting Information

XRD and UV–vis spectrum data of the ITO nanorod film, and SEM image and XRD data of the CIS/CdS/TiO_2/ITO film. This material is available free of charge via the Internet at http://pubs.acs.org/.

AUTHOR INFORMATION

Corresponding Author

*E-mail: bkmin@kist.re.kr (B.K.M.); yrdo@kookmin.ac.kr (Y.R.D.).

Notes

The authors declare no competing financial interest.

■ ACKNOWLEDGMENTS

This work is supported by the National Research Foundation of Korea Grant (NRF-2009-C1AAA001-0092935) funded by the Ministry of Education, Science and Technology. Also, the authors thank the program of the Korea Institute of Science & Technology (KIST).

■ REFERENCES

(1) Kemell, M.; Ritala, M.; Leskelä, M. *Crit. Rev. Solid State Mater. Sci.* **2005**, *30*, 1−31.
(2) Habas, S. E.; Platt, H. A. S.; van Hest, M. F. A. M.; Ginley, D. S. *Chem. Rev.* **2010**, *110*, 6571−6594.
(3) Mitzi, D. B.; Yuan, M.; Liu, W.; Kellock, A. J.; Chey, S. J.; Deline, V.; Schrott, A. G. *Adv. Mater.* **2008**, *20*, 3657−3662.
(4) Akhavan, V. A.; Goodfellow, B. W.; Panthani, M. G.; Reid, D. K.; Hellebusch, D. J.; Adachi, T.; Korgel, B. A. *Energy Environ. Sci.* **2010**, *3*, 1600−1606.
(5) Kaelin, M.; Rudmann, D.; Tiwari, A. N. *Sol. Energy* **2004**, *77*, 749−756.
(6) Lee, E.; Park, S. J.; Cho, J. W.; Gwak, J.; Oh, M.-K.; Min, B. K. *Sol. Energy Mater. Sol. Cells* **2011**, *95*, 2928−2932.
(7) Norsworthy, G.; Leidholm, C. R.; Halani, A.; Kapur, V. K.; Roe, R.; Basol, B. M.; Matson, R. *Sol. Energy Mater. Sol. Cells* **2000**, *60*, 127−134.
(8) Kapur, V. K.; Bansal, A.; Le, P.; Asensio, O. I. *Thin Solid Films* **2003**, *431−432*, 53−57.
(9) Yu, G.; Gao, J.; Hummelen, J. C.; Wudl, F.; Heeger, A. J. *Science* **1995**, *270*, 1789−1791.
(10) Coakley, K. M.; McGehee, M. D. *Chem. Mater.* **2004**, *16*, 4533−4542.
(11) Bach, U.; Lupo, D.; Comte, P.; Moser, J. E.; Weissörtel, F.; Salbeck, J.; Spreitzer, H.; Grätzel, M. *Nature* **1998**, *395*, 583−585.
(12) Wang, Q.; Zhu, K.; Neale, N. R.; Frank, A. J. *Nano Lett.* **2009**, *9*, 806−813.
(13) Pattantyus-Abraham, A. G.; Kramer, I. J.; Barkhouse, A. R.; Wang, X.; Konstantatos, G.; Debnath, R.; Levina, L.; Raabe, I.; Nazeeruddin, M. K.; Grätzel, M.; Sargent, E. H. *ACS Nano* **2010**, *4*, 3374−3380.
(14) Jang, W.; Kim, D.; Kim, J.; Min, B. K.; Kim, J.-D.; Yoo, K.-p. *Chem. Mater.* **2010**, *22*, 4350−4352.
(15) Yuhas, B. D.; Yang, P. *J. Am. Chem. Soc.* **2009**, *131*, 3756−3761.
(16) Krunks, M.; Kärber, E.; Katerski, A.; Otto, K.; Acik, I. O.; Dedova, T.; Mere, A. *Sol. Energy Mater. Sol. Cells* **2010**, *94*, 1191−1195.
(17) Liu, J.; Wang, S.; Bian, Z.; Shan, M.; Huang, C. *Appl. Phys. Lett.* **2009**, *94*, 173107.
(18) O'Hayre, R.; Nanu, M.; Schoonman, J.; Goossens, A. *Nanotechnology* **2007**, *18*, 055702.
(19) Lenzmann, F.; Nanu, M.; Kijatkina, O.; Belaidi, A. *Thin Solid Films* **2004**, *451−452*, 639−643.
(20) Guo, Q.; Ford, G. M.; Hillhouse, H. W.; Agrawal, R. *Nano Lett.* **2009**, *9*, 3060−3065.
(21) Panthani, M. G.; Akhavan, V.; Goodfellow, B.; Schmidtke, J. P.; Dunn, L.; Dodabalapur, A.; Barbara, P. F.; Korgel, B. A. *J. Am. Chem. Soc.* **2008**, *130*, 16770−16777.
(22) Park, J. H.; Park, H. K.; Jeong, J.; Kim, W.; Min, B. K.; Do, Y. R. *J. Electrochem. Soc.* **2011**, *158*, K131−K135.
(23) Yoo, B.; Kim, K.-J.; Bang, S.-Y.; Ko, M. J.; Kim, K.; Park, N.-G. *J. Electrochem. Soc.* **2010**, *638*, 161−166.